

## Research on the dehazing effect of orthogonal polarization method based on atmospheric scattering model and considering extinction ratio parameter

Dongdong Shi, Fuyu Huang, Leilei Jia, Yuandong Niu, Shuangyou Chen, Liting Jiao, Yanhua Huang & Limin Liu

**To cite this article:** Dongdong Shi, Fuyu Huang, Leilei Jia, Yuandong Niu, Shuangyou Chen, Liting Jiao, Yanhua Huang & Limin Liu (2024) Research on the dehazing effect of orthogonal polarization method based on atmospheric scattering model and considering extinction ratio parameter, International Journal of Remote Sensing, 45:5, 1556-1573, DOI: [10.1080/01431161.2024.2314006](https://doi.org/10.1080/01431161.2024.2314006)

**To link to this article:** <https://doi.org/10.1080/01431161.2024.2314006>



Published online: 15 Feb 2024.



Submit your article to this journal [↗](#)



Article views: 4



View related articles [↗](#)



View Crossmark data [↗](#)



# Research on the dehazing effect of orthogonal polarization method based on atmospheric scattering model and considering extinction ratio parameter

Dongdong Shi<sup>a,b</sup>, Fuyu Huang<sup>a</sup>, Leilei Jia<sup>a</sup>, Yuandong Niu<sup>a</sup>, Shuangyou Chen<sup>a</sup>,  
Liting Jiao<sup>a</sup>, Yanhua Huang<sup>b</sup> and Limin Liu<sup>a</sup>

<sup>a</sup>Shijiazhuang Campus, Army Engineering University of PLA, Shijiazhuang, PR China; <sup>b</sup>Department of General Education, Army Engineering University of PLA, Nanjing, PR China

## ABSTRACT

The hazy weather is currently one of the most common atmospheric environments. It is an urgent problem to realize clear imaging in hazy environment. Orthogonal polarization dehazing is one of the classical dehazing techniques attracting a widespread attention from research workers. However, while using this method, the extinction ratio ( $ER$ ) parameter of the polarizer was neglected leading to poor dehazing. Therefore, we have introduced the  $ER$  of polarizers into the orthogonal polarization dehazing technique in this paper. In the process of sky region division, this study proposes to use HSV, RGB and Lab colour channels to create a comprehensive mask to select the sky region. And the morphological corrosion operation is utilized to increase the region connectivity for better sky region division. Based on subjective visualization, it can be found that the dehazing effect is significantly enhanced with the introduction of  $ER$ . The dehazing effect was evaluated based on four parameters of contrast ( $C_0$ ), peak signal-to-noise ratio ( $PSNR$ ), structural similarity index measure ( $SSIM$ ) and information entropy ( $E_n$ ). It is further demonstrated the necessity of introducing  $ER$ . The experimental results show that the  $ER$  can make the dehazing effect of the orthogonal polarization dehazing technique improved, which is valuable for the engineering application of image processing in hazy environment. The experimental results proved to be encouraging.

## HIGHLIGHTS

- The main highlights of this work are the following three points:  
The NDC parameter of the polarizer is a crucial factor that many researchers tend to overlook when utilizing polarizers for detection in the polarization dehazing process. This study aims to address this oversight by incorporating polarizers for detection and introducing the NDC parameter to rectify images at varying polarization angles. Consequently, the polarization dehazing operation yields superior results compared to those achieved without NDC polarization dehazing technology.

## ARTICLE HISTORY

Received 23 October 2023  
Accepted 22 January 2024

## KEYWORDS

Polarization-based dehazing;  
extinction ratio; algorithm  
research; image processing

- The separation of the sky area from the non-sky area is achieved through the utilization of a multi-channel mask. This model employs multi-channel processing, specifically the HSV colour channel, RGB colour channel, and Lab colour channel. By generating an appropriate mask to delineate the sky area and the non-sky area, merging the three masks into a comprehensive mask, and subsequently applying morphological etching on the comprehensive mask to enhance the connectivity of the sky area, it is observed that the effectiveness of separating the sky area from the non-sky area is significantly improved.
- The amalgamation of image restoration and image enhancement is a critical process. Once the polarization dehazing operation is accomplished, we proceed with an image enhancement operation on the restored image. To regulate the filtering level, we employ the standard deviation of the Gaussian function. Furthermore, we utilize the Laplacian operator to intensify the edges of the current channel. By adjusting the parameters, we can control the intensity and scope of the enhancement effect, thereby achieving edge enhancement and augmenting the details of the image.

## 1. Introduction

Complex and severe weather, such as precipitation, storms, smoke and haze, which can cause serious interference with the detection system, are significant factors in the blurring of imaging distortions or data anomalies. In hazy environment, target details in the detected image or video are severely lost, which hinders autonomous driving, outdoor surveillance and military reconnaissance. In particular, with increasing pollution in cities, haze-type weather has become the most common type of weather, often causing traffic jams and threatening lives and properties. Therefore, the research on this kind of weather has also drawn a lot of attentions (Liang et al. 2016; Schechner, Narasimhan, and Nayar 2003; X. Wang et al. 2019). Optical detection systems have become the dominant method of detection nowadays due to their high imaging resolution, wide range of instruments, richness of information and accuracy. In a hazy environment, the atmosphere is full of aerosols of different sizes, dust particles, etc., which causes a large amount of target information to be lost and feature details to be blurred. It is seriously affected the subsequent image analysis and understanding. The reason of this is that the light in the hazy environment is seriously absorbed and scattered by the light mist produced by particles such as dust or water (Hautiere et al. 2008; Huang et al. 2015; Mudge and Virgen 2013). The scattering effect caused by these air molecules is the primary factor that converts natural light into polarized light (Narasimhan and Nayar 2002). The polarization pattern has a certain distribution pattern, and this polarization pattern is one of the important properties for the atmosphere.

It is now clarified that in hazy environments, image degradation is mainly considered in the following three points. firstly, attenuation of target information. Secondly, atmospheric optical noise. Thirdly, scattering blurring of target imaging. To address the image degradation problem, many researchers have conducted in-depth explorations and proposed various removal methods and removal models. The dehazing methods for

images can be mainly categorized into two types: image enhancement and restoration (Hautiere et al. 2008). Image enhancement techniques are effective but poorly targeted under the whole, by highlighting the target to remove non-target information enhance the contrast, so as to reach the visualization of the haze map. Typical schemes for such techniques include the Retinex algorithm (W. Wang et al. 2008; Zhuang, Li, and Wu 2021), the interpolated histogram equalization algorithm (Dar and Mittal 2021; Sengupta, Biswas, and Gupta 2020), and the CLAHE algorithm (Soni and Mathur 2020), among others. Image restoration technique is a physical model-based scheme to analyse the effect of hazy weather on images. Its restoration effect is closer to the real scene. In the domain of image restoration techniques, there exists a broad spectrum of methods that can be employed. An instance of such a technique is the Oakley model, which utilizes gradients and image depth to formulate a differential equation-based approach that facilitates the extraction of depth information that is tailored to the target (Oakley and Satherley 1998). Additional techniques involve employing models for atmospheric transmission functions (Buckley and Hogan 2017; Sun and Xiang 2020) and atmospheric scattering models (Ju, Zhang, and Wang 2016; Qu and Zou 2017), among others. In recently years Kaiming H proposed the dark channel a priori dehaze algorithm based on the model of atmospheric scattering physics and the inverse operation according to the formation process of foggy images, after which the dehaze technology has been developed rapidly (He, Sun, and Tang 2011). Asem Khmag estimates the transmission map based on L2-parameters and then enhances the transmission map of the estimated resultant image using second generation wavelet transform filter. It is proposed a single image fast haze removal technique based on edge and fine texture preservation (Khmag 2023; Khmag et al. 2017).

On this basis, polarization detection has the advantages of simplicity of operation and moderate cost. By using the polarization property of scattered light. Schechner et al. proposed the polarization dehazing scheme, which is a method of atmospheric light estimation that can achieve rapid dehazing by using the atmospheric scattering model and the fact that the atmosphere is partially polarized in hazy environment (Schechner, Narasimhan, and Nayar 2001). Polarization dehazing technology is now being rapidly developed, typically polarization differential dehazing (J. Wang et al. 2022; Zhu et al. 2015), Stokes vector polarization dehazing (Rubin et al. 2019; Vedel, Breugnot, and Lechocinski 2011; Y. Wang et al. 2022), and deep learning dehazing (Bindu, Sidhu, and Jyoti 2017; Chen et al. 2022; Sharma, Kumar, and Singla 2021). It is obtained the polarization parameter in the model, which leads to the dehaze effect.

At present, although there are many processing schemes, the advantages and disadvantages of each scheme coexist. It is not possible to satisfy that all the variables are optimal solutions, and the implementation of the scheme has different focuses. Therefore, in practical application, it needs to be modified according to different scenarios. This paper is based on the atmospheric scattering model theory to carry out the work, and the polarization classification is based on the polarization characteristics of the atmospheric scattered light and the target attenuated transmitted light. Then the polarization detection theory is used to synthesize the three main factors of image degradation in hazy environments. The dehazing effects of orthogonal polarization dehazing with the introduction of the extinction ratio parameter ( $ER$ ) are compared with those of orthogonal polarization dehazing without the introduction of the  $ER$ , and quantitative evaluation data are given for judging.



## 2. Experimental procedures and methods

It has been demonstrated that the scattering coefficient and wavelength don't correlate well in the visible wavelength band (Menglei et al. 2023). In the hazy environment, reflected light from the target and sunlight are captured by our imaging system through atmospheric scattering. As shown in Figure 1(a), the total energy captured by our imaging system can be divided into two parts depending on the source: atmospheric scattered light  $A$  and transmitted light  $D$  attenuated by the target through the atmosphere. After the light is scattered by multiple scattering of atmospheric particles, the scattering direction is random and shows exponential attenuation with increasing detection distance. And the polarization is inversely proportional to the number of scattering. Therefore, the concentration of fog increases, the scattering probability increases, and the deskewing effect increases with it (Treibitz and Schechner 2009). If the degree of polarization ( $DoP$ ) in the atmospheric scattered light  $A$  reaches a certain threshold, polarization dehaze can be performed by using  $DoP$ . The research idea in this paper is the same as Schechner's assumption that the atmospheric scattered light  $A$  contains partially polarized light (Schechner, Narasimhan, and Nayar 2001). For the target transmitted light  $D$  the polarization characteristics of the light emitted from the scene target do not change due to the hazy environment for long-range imaging.

Therefore, the total light intensity collected can be decomposed into (Liu et al. 2016; Schechner, Narasimhan, and Nayar 2001):

$$I_{total}(x, y) = A(x, y) + D(x, y) = A_p(x, y) + A_{no-p}(x, y) + D(x, y) \quad (1)$$

Where  $A_p$  is the polarized component of  $A$ .  $A_{no-p}$  refers to the non-polarized component of  $A$ .  $(x, y)$  represents the position in the image.

In this dehazing model, as  $A$  is decomposed into polarized and unpolarized components, it is mathematically necessary to separate the two components in order to represent the polarization characteristics of  $A$  accurately. A polarizer is installed on the camera to acquire images in two mutually orthogonal directions by employing rotational manipulation. It is crucial to acknowledge that as the polarizer undergoes rotation,  $I_{total}$  demonstrates a cosine function trend relative to the angle of the polarizer. Consequently, the

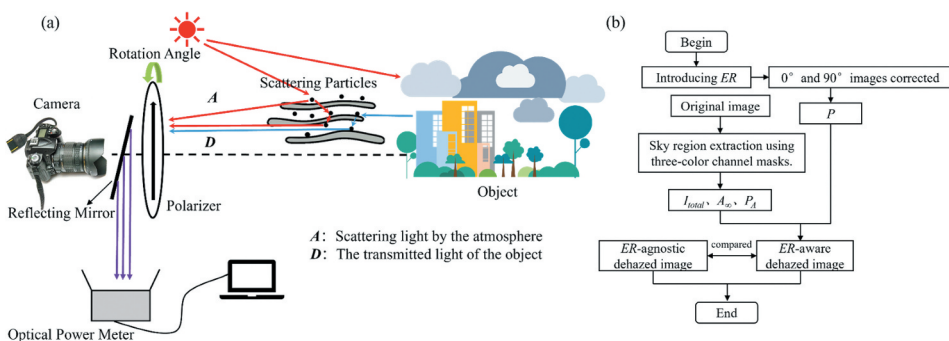


**Figure 1.** Method overview: (a) Presents a schematic illustration of atmospheric scattering in hazy environmental conditions, (b) Research framework.

intensity of light received by the detector's photosensitive unit was assessed by using the following:

$$\begin{aligned} I_{\max}(x, y) &= A_{\max}(x, y) + \frac{D(x, y)}{2} \\ I_{\min}(x, y) &= A_{\min}(x, y) + \frac{D(x, y)}{2} \end{aligned} \quad (2)$$

Where  $I_{\max}(x, y)$  represents the maximum light intensity received at each pixel point in the image, while  $I_{\min}(x, y)$  corresponds to the minimum value. Likewise,  $A_{\max}(x, y)$  and  $A_{\min}(x, y)$  are associated with the maximum and minimum values, respectively.

It is crucial to acknowledge that the assumption of an ideal state for the polarizer in Equation (2) neglects the presence of extinction ratio parameters, which often go unnoticed by researchers in practical applications. To address this issue, this work introduces a new parameter called the extinction ratio parameter, denoted as  $ER$ , into the calculation process. Considering the variability of the  $ER$  from the labelled value under different conditions of use of the polarizer. Consequently, a reflector was first placed in front of the camera, and the value on the illuminance metre was observed during the rotation of the polarizer (Instrument types: HIOKI FT3424, Japan, illumination measurement range: 0.00–200000 lx, experimental: 2000 lx). The angles of the polarizing filter at which the maximum and minimum values of illuminance metre were recorded are noted as  $\theta_{\max}$  and  $\theta_{\min}$ , respectively. Actual measurements have verified that  $\theta_{\max} - \theta_{\min}$  is approximately equal to  $90^\circ$ . Hazy weather images are captured under two conditions: without a polarizing filter and with the polarizing filter set at angles  $\theta_{\max}$  and  $\theta_{\min}$ , respectively. The light intensity at each pixel in the image is meticulously measured and documented as  $I_{00}$  and  $I_{90}$ . The correction process is derived from Equations (3,4):

$$ER = 10 \cdot \log_{10} \frac{I_{00}}{I_{90}} \quad (3)$$

Here the correction is applied to each of the R, G and B channels of the image, with  $ER$  refers to the extinction ratio. The  $ER$  is then used to correct each pixel point of the original image:

$$\begin{aligned} I_{00}^{\text{correct}} &= I_{00} - ER \\ I_{90}^{\text{correct}} &= I_{90} + ER \\ I_{\text{total}}^{\text{correct}} &= I_{00}^{\text{correct}} + I_{90}^{\text{correct}} \end{aligned} \quad (4)$$

Where  $I_{00}^{\text{correct}}$  and  $I_{90}^{\text{correct}}$  are the gray values of the image pixel points at the corrected polarizer rotation angles  $\theta_{\max}$  and  $\theta_{\min}$ , respectively. The polarization degree  $P$  of the corrected image as well as the whole environment is:

$$P = \frac{I_{00}^{\text{correct}} - I_{90}^{\text{correct}}}{I_{00}^{\text{correct}} + I_{90}^{\text{correct}}} \quad (5)$$

It is clarified here that all the calculation processing that follows refers to the grey scale order of the image pixel points. According to the intensity of light in the sky region in the  $0^\circ$  and  $90^\circ$  images, the polarization of the atmospheric scattered light,  $P_A$ , can be obtained:

$$A_{\infty}^{correct} = A_{\infty}^{00,correct} + A_{\infty}^{90,correct}$$

$$P_A = \frac{A_{\infty}^{00,correct} - A_{\infty}^{90,correct}}{A_{\infty}^{00,correct} + A_{\infty}^{90,correct}}$$

The atmospheric light intensity at infinity or extreme distance, denoted by  $A_{\infty}^{correct}$ , is a crucial factor to consider.  $A_{\infty}^{00,correct}$  and  $A_{\infty}^{90,correct}$  represent the atmospheric light intensity at infinity collected by corrected polarizers taken perpendicular to each other, respectively. It is important to note that the intensity of atmospheric scattered light,  $A$ , increases as the scattering distance,  $d$ , increases. The calculations and processing conducted in this study specifically focus on the grayscale levels of the image pixels (Liu et al. 2016):

$$A_{correct} = A_{\infty}^{correct}(1 - e^{-\beta d}) \quad (7)$$

The atmospheric scattering factor, denoted as  $\beta$ , plays a crucial role in the process of estimating the radiance intensity of a target scene by compensating for the atmospheric light noise. By utilizing the transfer function, it can be observed that the total radiance, denoted as  $A_{\infty}^{correct}$ , is inversely related to the detection distance,  $d$ . Consequently, the radiance information of the target scene can be expressed in the following manner.

$$D_0 = I_{total}^{correct} \left( 1 - \frac{P}{P_A} \right) \left( \frac{A_{\infty}^{correct} P_A}{A_{\infty}^{correct} P_A - I_{total}^{correct} P} \right) \quad (8)$$

Based on Equation (8), the essential variables for the restoration of haze scenes are  $P$ ,  $P_A$ , and  $A_{\infty}^{correct}$ . The value of  $P$  can be derived by evaluating the intensity images taken at two different angles, specifically  $0^\circ$  and  $90^\circ$ . By capturing images in these two directions and calculating the disparity between them, it becomes possible to determine the value of  $P$ . This value of  $P$  facilitates the estimation of the energy transmission ratio in the haze scene, thereby allowing for the restoration of a clear image. In practical implementation, the accurate computation of  $P$  for the purpose of haze scene restoration can be accomplished by measuring these images and applying suitable processing techniques.

In the process of estimating the atmospheric light intensity at infinity, a method is employed which involves the segmentation of the sky area from the non-sky area. Through this differentiation, it becomes possible to identify the pixel within the sky area that possesses the highest greyscale value, which can then be utilized as an estimation of the atmospheric light intensity at infinity. To achieve this goal, image segmentation techniques are utilized in order to effectively separate the sky and non-sky areas. This enables a focused analysis of the intensity values of the pixels within the sky area. By selecting the pixel with the maximum greyscale value within the sky area, an estimation of the atmospheric light originating from an infinite distance can be obtained. This estimation is based on the Equation (8) and the transfer function,  $d \rightarrow \infty$ ,  $D \rightarrow 0$ :

$$I_{total}^{correct} = D_0 e^{-\beta d} + A_{\infty}^{correct}(1 - e^{-\beta d}) \rightarrow A_{\infty}^{correct} \quad (9)$$

The resulting difference represents the polarization impact caused by the atmospheric light. To obtain accurate  $P_A$  values, it is recommended to normalize these differences with the atmospheric light intensity. Additionally, in order to minimize potential errors resulting from variations in individual data during the computation of  $A_{\infty}^{correct}$  for each pixel. It is

advisable to sort the atmospheric light intensity values in ascending order and consider only the last 20% of the data for averaging. This approach effectively reduces the influence of outlier values and improves the precision of the calculation.

### 3. Results and discussions

#### 3.1. Introducing *ER*

The study involved the implementation of three photography sets, which consisted of capturing images on a hazy day without a polarizer, along with images taken using a polarizer set at angles of  $0^\circ$  and  $90^\circ$ . It is worth noting that the distance between the shooting location and the distant buildings was estimated to be approximately 4.7 km based on the map. The haze day images obtained at both  $0^\circ$  and  $90^\circ$  angles were subjected to optimization using the *ER* parameter. Furthermore, these images were subsequently restored to their initial colour representation.

As shown in Figure 2, comparing Figure 2(a–d) respectively, the difference in brightness can be clearly found. The light intensity was attenuated or enhanced during the correction process. It is shown that the error produced by not considering the *ER* on

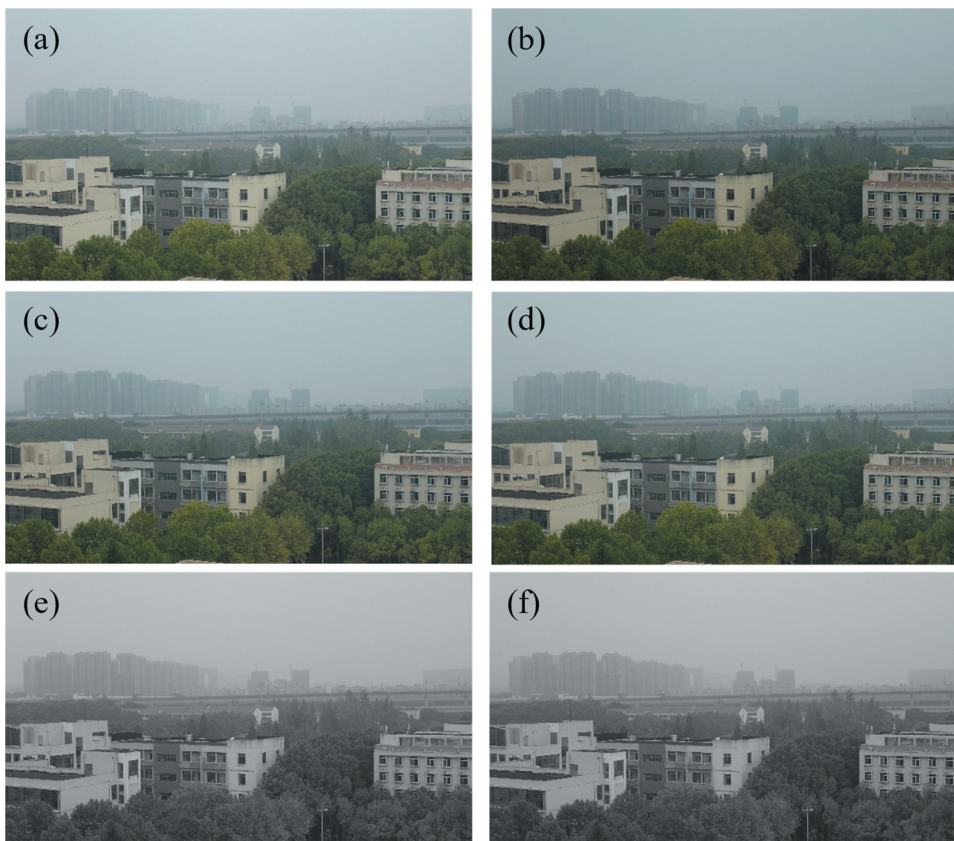


**Figure 2.** The images were subjected to correction using the *ER*: (a, b) Images captured at  $0^\circ$  and  $90^\circ$ , (c, d) the corrected images at  $0^\circ$  and  $90^\circ$ , (e, f) the corrected greyscale images at  $0^\circ$  and  $90^\circ$ .

polarization imaging. The polarization dehazing effects with and without considering  $ER$  will be given later, further proving the conjecture. Figure 2(e,f) show the greyscale maps corresponding to the  $0^\circ$  and  $90^\circ$  hazy sky images after correction. The greyscale processing is performed for RGB three-channel colour recovery.

### 3.2. Sky area identification

In order to estimate the intensity of atmospheric light from a distant point, it is crucial to distinguish the sky region from the target scene. To achieve this, a multi-channel approach involving the HSV, RGB, and Lab colour channels is proposed for identifying the sky area. By adjusting the threshold ranges of these colour channels, masks are created to designate the sky and non-sky areas. These masks are then combined into a single mask:

$$M_{\text{merge}(x,y)} = M_{\text{HSV}(x,y)} \& M_{\text{RGB}(x,y)} \& M_{\text{Lab}(x,y)} \quad (10)$$

The masks denoted as  $M_{\text{HSV}(x,y)}$ ,  $M_{\text{RGB}(x,y)}$ , and  $M_{\text{Lab}(x,y)}$  represent the colour channel masks for HSV, RGB, and Lab respectively.

The combined mask is subjected to morphological erosion operations to improve the connectivity of the sky area. By modifying the shape and size of the structuring element used in the erosion operation, the area selection process can be enhanced, removing small noise and effectively connecting adjacent pixel areas. Consequently, a more comprehensive extraction outcome of the hazy sky area can be achieved. In this research, we employ the morphological 'disk' erosion operation – a technique that utilizes circular structural elements – to achieve multiple objectives. This operation not only ensures the refinement of image object edges, but also facilitates the reduction and segmentation of objects within an image:

$$T_{fs} = T_0 ! Z \quad (11)$$

$T_0$  represents the initial image.  $!$  signifies the process of corrosion.  $Z$  symbolizes a circular structural component.  $T_{fs}$  refers to the image affected by corrosion.

The sky region is indicated by the colour red, while the non-sky region is marked in black, the recognition results are shown in Figure 3. It can be found that the main part of the sky region of the original,  $0^\circ$  and  $90^\circ$  images is basically recognized. The outline information of distant buildings is more complete, and the region is not mis-selected due to the influence of the hazy environment. The influence of individual very small region mis-selection on the calculation results can be ignored, and the recognition results are highly credible. It proved to be feasible to complete the separation of the sky region by using the masks of the three colour channels to form a composite mask.

The successful introduction of extinction ratio  $ER$  and the recognition processing of the sky region has been accomplished, and the acquisition of  $D_0$  on the three channels of  $P_A$  and RGB can be accomplished based on the grey values of the corrected image and the sky region. To visually assess the spatial distribution of  $P_A$  values across the image, a colour mapping chart was created. The successful calculation of  $P_A$  using the entire sky area is demonstrated in Figure 4, with notable effects. However, noise interference was encountered at the boundary between the sky area and non-sky area, leading to higher  $P_A$  values. Upon

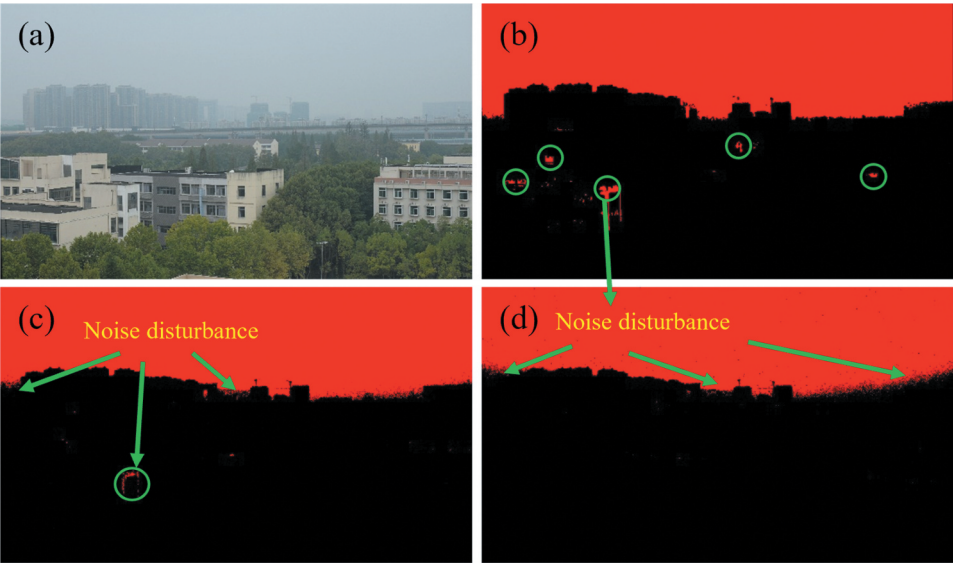


**Figure 3.** The identification effect of the sky area: (a) Original image, (b-d) Sky area identification effect of original, 0° and 90° images.

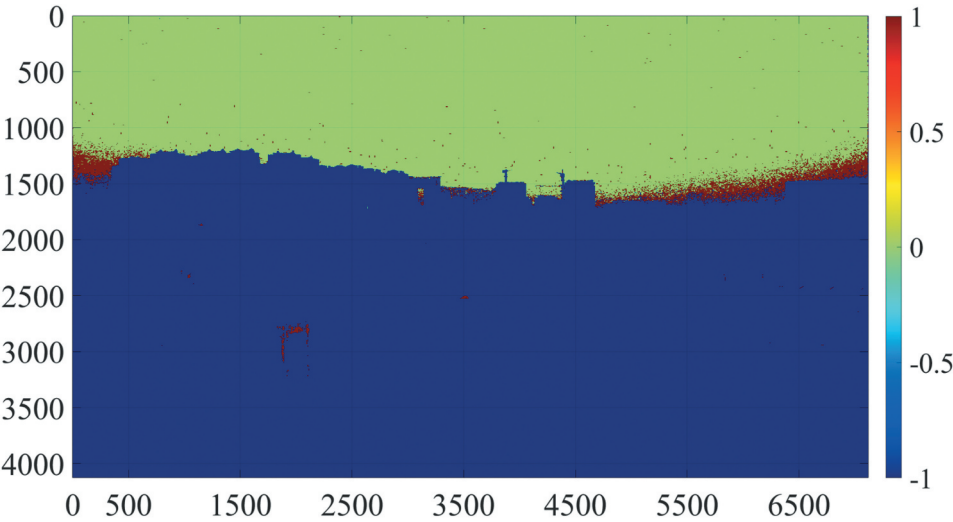


**Figure 4.** The colour mapping chart of  $P_A$ .

inspecting the  $P_A$  matrix of the sky area, it was observed that the values consistently exhibited stability, providing additional support for the random nature of atmospheric scattering and confirming the validity of our assumptions. To minimize noise disturbances at the boundaries, the elements of the  $P_A$  matrix of the entire sky area were sorted in ascending order. Subsequently, values within the 70–80% range were selected, and their average was computed, resulting in a  $P_A$  value of 0.2065.



### 3.3. Comparison of polarization dehazing effect

Based on the  $I_{total}^{correct}$  of each pixel in the original haze image and the Equation (8), it can be observed that the atmospheric scattering is selective with respect to the wavelength. Furthermore, the polarization characteristics vary across different colour channels. Consequently, image processing is carried out on the three RGB channels, and the resulting channels are merged using the cat function. By considering the  $ER$  parameter, polarization dehazing images are obtained, as well as polarization dehazing images without considering the  $ER$  parameter. In order to evaluate the dehazing effectiveness from the objective point of view, four kinds of evaluation of dehazing capability are used, including the contrast ( $C_0$ ) parameter between the scene target and the sky background, the peak signal-to-noise ratio ( $PSNR$ ), the structural similarity index measure ( $SSIM$ ), and the information entropy ( $E_n$ ) (Qi et al. 2015).

Since the background grey scale is much larger than the grey scale of the scene target. It is possible to use an improved method of calculating the  $C_0$  between the scene target and the sky background:

$$C_0 = \frac{|G_S - G_B|}{\min(G_S, G_B)} \quad (12)$$

Where  $G_S$  represents the mean grey value of sky area in the image, while  $G_B$  corresponds to the mean grey value of scene target of non-sky area.

The  $PSNR$  and the mean square error ( $MSE$ ) are defined:

$$PSNR = 20 \times \lg\left(\frac{255}{\sqrt{MSE}}\right) \quad (13)$$

$$MSE = \frac{1}{H \times W} \sum_{i=1}^H \sum_{j=1}^W [X(i,j) - Y(i,j)]^2$$

Where  $MAX$  represents maximum value of image signal.  $MSE$  depicts the image mean square error.  $H$  and  $W$  represent the length and width of image  $X$  and image  $Y$ .

$SSIM$  is defined as:

$$SSIM(X, Y) = \frac{(2\mu_X\mu_Y + C_1)(2\sigma_{XY} + C_2)}{(\mu_X^2 + \mu_Y^2 + C_1)(\sigma_X^2 + \sigma_Y^2 + C_2)} \quad (14)$$

Where  $\mu_X$  and  $\mu_Y$  represent the mean of the images  $X$  and  $Y$ .  $\sigma_X$  and  $\sigma_Y$  denote the mean variance.  $\sigma_{XY}$  denotes the covariance.  $C_1$  and  $C_2$  are constants.

$E_n$  is defined as:

$$E_n = - \sum_{i=0}^{L-1} p(i) \log_2 p(i) \quad (15)$$

Where  $L$  represents the full greyscale image,  $p(i)$  depicts the ratio of the grey value of  $i$  to the full pixels of the image.

The comparison between the original image and the two polarization-based dehazed images is illustrated in Figure 5(a,c,e). It is evident that the dehazing effect is significant regardless of the consideration of  $ER$ . Upon closer inspection, it is clear that the dehazing effect, when considering the  $ER$ , outperforms the dehazing effect without considering it. The

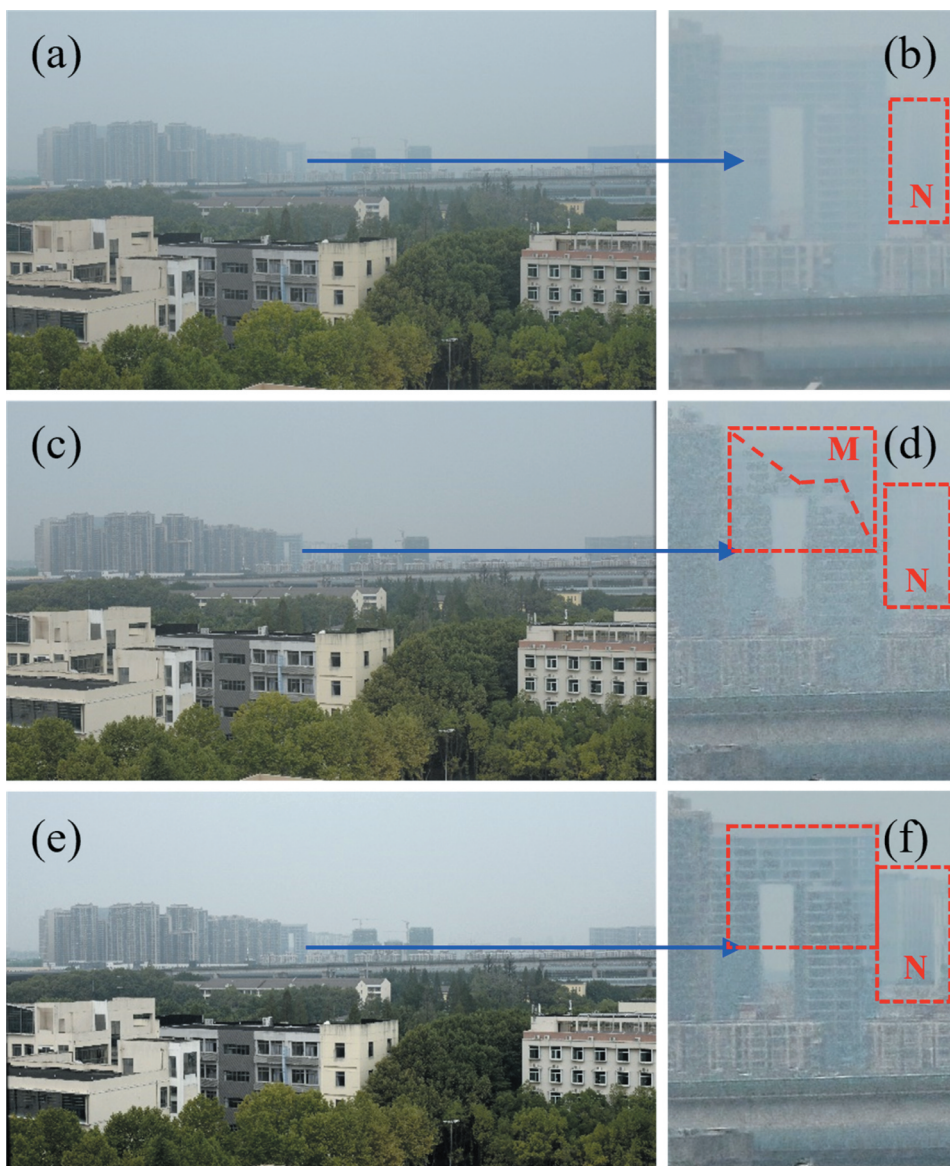


**Figure 5.** The comparison of polarization-based dehazed images: (a,c,e) original image, *ER*-agnostic dehazed image, *ER*-aware dehazed image, (b,d,f) the zoomed-in image.

contrast is notably increased at various floor levels, resulting in a clearer depiction of the overall architectural contours. However, in the upper-right corner of the selected area M in Figure 5(d), the dehazing effect is less noticeable. This can be attributed to two main reasons. Firstly, the selected area M is situated near the boundary between the sky and the target scene, which introduces substantial noise disturbance and blurs the area's demarcation. Secondly, the images captured at  $0^\circ$  and  $90^\circ$  have not undergone photometric correction, leading to undesirable implications such as brightness distortion, reduced contrast, colour misalignment, and information loss in the resulting coloured imagery. In contrast, the



dehazing effect at the same position in Figure 5(f) is better, indicating that the introduction of  $ER$  can enhance image quality and preserve more details and information. Consequently, image correction prior to dehazing is necessary. Next, in order to evaluate the dehaze effect on distant buildings, we compare the conventional orthogonal polarization dehaze technique without introducing  $ER$  with our method. As shown in the N region in Figure 5(b,d,f), it can be clearly found that the dehazing effect of not considering  $ER$  for further away is average, the haze noise is hardly removed and the building information is not recovered. However, after introducing the  $ER$  parameter, the building information in the N region is recovered. Therefore, the introduction of  $ER$  has better scene information recovery capability.

To further characterize the demisting effect of  $ER$  on the orthogonal polarization method, quantitative evaluation data for the four demisting techniques,  $C_0$ ,  $PSNR$ ,  $SSIM$ , and  $E_n$ , are present in Table 1. The  $C_0$  between the scene target and the background of the sky region goes from 0.6105 (haze-free) to 0.2417 ( $ER$ -agnostic) to 0.5218 ( $ER$ -aware). The  $SSIM$  data is a comprehensive judgement of three key feature information: brightness, contrast and structure before and after dehazing. It can be found that the introduction of  $ER$  results in  $SSIM$  values that are 0.2801 higher compared to the non-introduction of  $ER$ . Meanwhile, the two dehazed images are compared with the haze-free image for  $SSIM$ , and the result is shown in Figures 6(a,b). It can be clearly found that after the introduction of  $ER$ , the contrast and details of the image are improved, and the structure of the target is clearer. Higher the  $E_n$ , clearer the image. When without haze,  $E_n$  is 8.5798; when no  $ER$  is introduced,  $E_n$  is 7.2307; after  $ER$  is introduced,  $E_n$  is 7.4048. Based on the values of the four quantitatively evaluated parameters, it is shown that the  $ER$  of the polarizer has an important role in the orthogonal polarization method of dehazing technique, which can greatly improve the dehazing effect of the orthogonal polarization method.

In order to evaluate the effect of the orthogonal polarization method dehazing algorithm with the introduction of  $ER$ . The RGB distribution of each pixel point of the image and the grey value of the image with respect to the number of pixels are given. However, when considering the  $ER$  polarization dehazing image, the

**Table 1.** Quantitative assessment of two techniques on haze removal images.

	$C_0$	$PSNR$ (dB)	$SSIM$	$E_n$
Haze-free image	0.6105	-	-	8.5798
$ER$ -agnostic dehazed image	0.2417	71.59	0.7630	7.2307
$ER$ -aware dehazed image	0.5218	78.25	0.8900	7.4048

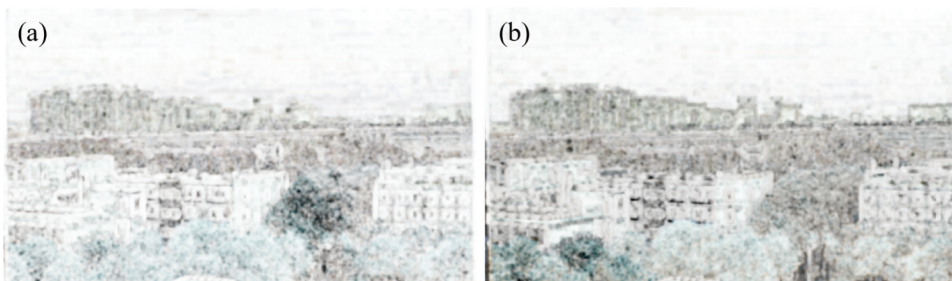


**Figure 6.** Comparison of  $SSIM$ : (a)  $ER$ -agnostic, (b)  $ER$ -aware.

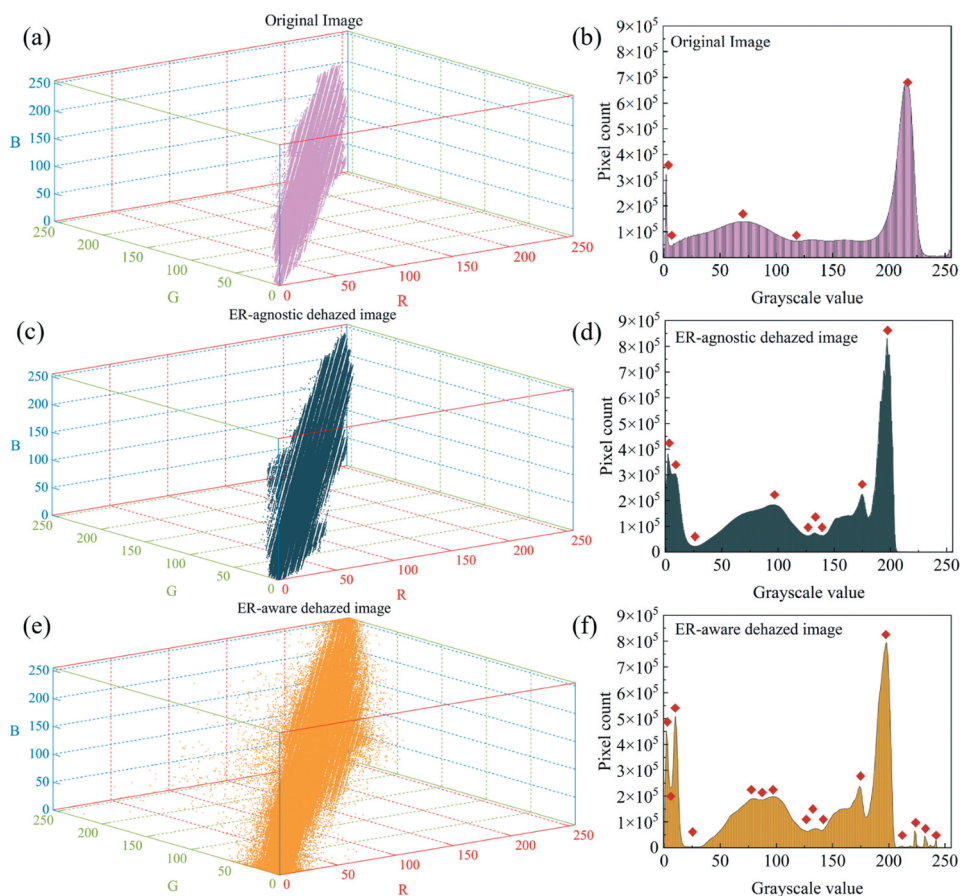


**Figure 7.** Evaluation of polarization dehazing effect: (a,c,e) RGB distribution of each pixel, (b,d,f) Grayscale value vs Pixel count.

colour distribution becomes gradually dispersed, indicating a richer colour information that closely resembles the real scene. Additionally, upon examining Figure 7(b), it becomes evident that the relationship curve between the grey value of the original image and the number of pixels has only a small number of extreme points. These extreme points are clearly marked in Figure 7(b,d,f). Notably, in Figure 7(d,f), the number of extreme points in the curve significantly increases, highlighting the pronounced impact of the *ER* polarization dehazing algorithm. Comparing the haze-free images without *ER* enhancement to the haze images, the number of extreme points in the former increases by 100%. However, with the introduction of *ER* enhancement, the number of extreme points experiences a remarkable increase of 220%. This enhancement results in an improved contrast between the target and both the target-background and target-object in the image. Consequently, it further validates the significant improvement effect of *ER* on polarization dehazing imaging.

### 3.4. Image edge enhancement

The polarization dehazing algorithm with *ER* has been chosen for the purpose of obtaining an image that contains a more comprehensive representation of the scene. To further enhance the dehazed image, it becomes imperative to improve the resolution of details and the contrast of contours pertaining to the target. The level of filtering, which directly impacts the degree of image smoothing, can be regulated by finely tuning the standard deviation parameter  $\sigma$  of the Gaussian function, taking into account the varied polarization characteristics exhibited by each channel. Subsequently, the Laplacian operator is employed to augment the edge of the current channel, with the intensity and extent of the enhancement effect being adjustable. The horizontal difference of the image pixel is denoted as  $D_x$ , whereas the vertical difference is expressed as  $D_y$ . Accordingly, the second derivative of the dehazing image  $f(x,y)$  can be expressed as follows:

$$\begin{aligned} D_{xx} &= f(x+1, y) - 2f(x, y) + f(x-1, y) \\ D_{yy} &= f(x, y+1) - 2f(x, y) + f(x, y-1) \end{aligned} \quad (16)$$

It can be mathematically represented as the summation of the second-order derivatives in both the horizontal and vertical directions based on the definition of the Laplacian operator:

$$L(x, y) = D_{xx} + D_{yy} \quad (17)$$

In this particular context, we utilize the discrete version of the Laplacian operator of a template size measuring  $3 \times 3$ . By applying the Laplacian operator to this specific neighbourhood, we compute the gradient or edge magnitude at each individual pixel. The identification of areas within an image that contain edges is of utmost importance during the execution of edge detection. At the edges, the Laplacian operator generates notable responses owing to the abrupt change or discontinuity in pixel values. Consequently, by precisely locating the zero-crossings of the Laplacian operator, it becomes feasible to accurately determine the positions of the edges.

The results of the image enhancement, as shown in [Figure 8](#), exhibit significant advancements in the clarity and visual quality of the enhanced buildings. Specifically, [Figure 8\(b,d\)](#) demonstrate that the enhanced images possess improved sharpness, with more pronounced contours and enhanced edge details. Moreover, the low-contrast areas exhibit effectively enhanced contrast, resulting in a more vibrant and detailed appearance. It is important to note that the colour accuracy remains intact throughout the enhancement process. Additionally, there is a 17% increase in contrast between the building target and the sky background after enhancement. Consequently, utilizing the Laplacian matrix as the edge for enhancing the current channel in the dehazing problem proves to be effective. In practical applications, it is advisable to employ a combined approach of image restoration and enhancement techniques, as it significantly enhances both the clarity and visual appeal of dehazed images.

## 4. Conclusions

In this study, the extinction ratio parameter *ER* is introduced to modify the conventional orthogonal polarization method. Then, the modified orthogonal polarization



**Figure 8.** Image enhancement outcome: (a) *ER*-aware dehazed image, (c) enhanced image, (b,d) the zoomed-in image.

technique is utilized for dehazing. In sky region selection, three different masks are utilized to form a composite mask, which is separated to obtain accurate sky region. According to the characteristic that scattering is selective to the wavelength, polarization dehaze is performed for the R, G and B channels respectively. With the new orthogonal polarization haze removal technique, the contrast between the distant buildings and the background is significantly improved. The information about the buildings is refined, and high-quality images are produced. Four parameters,  $C_0$ ,  $PSNR$ ,  $SSIM$  and  $E_n$ , are utilized to quantitatively evaluate the traditional and new methods. It is further demonstrated that *ER* has a non-negligible effect on the haze removal effect of the orthogonal polarization method. Finally, by utilizing image enhancement techniques, the detail information is greatly improved and the edge information is richer. The enhancement increases the contrast between the building targets and the background of the sky area by 17%. The achievement can be applied to the mid- and long-distance hazy environments. If combined with a high-quality lens can be realized long-distance polarization to remove the haze, the haze removal effect will be further improved.

### Disclosure statement

No potential conflict of interest was reported by the author(s).

## Funding

The work was supported by the National Natural Science Foundation of China [62171467]; Natural Science Foundation of Hebei Province [F2021506004].

## Author agreement

The all authors certify that have seen and approved the final version of the manuscript being submitted. We warrant that the article is our original work, hasn't received prior publication and isn't under consideration for publication elsewhere.

## Credit authorship contribution statement

**Dongdong Shi:** Funding acquisition, Project administration, Supervision, Conceptualization, Software, Writing-original draft, Writing-review & editing. **Fuyu Huang:** Methodology, Investigation. **Leilei Jia, Yuandong Niu, Shuangyou Chen & Liting Jiao:** Data curation. **Yanhua Huang:** Conceptualization, Resources, Visualization, Validation. **Limin Liu:** Supervision, Writing-review, Formal analysis.

## Data statement

The data that support the findings of this study are available from the corresponding author, [Limin Liu], upon reasonable request.

## References

- Bindu, B., J. S. Sidhu, and K. Jyoti. 2017. "A Review of Image Restoration Based Image Defogging Algorithms." *International Journal of Image, Graphics and Signal, Processing* 9 (11): 62–74. <https://doi.org/10.5815/ijigsp.2017.11.07>.
- Buckley, D. T., and C. J. Hogan. 2017. "Determination of the Transfer Function of an Atmospheric Pressure Drift Tube Ion Mobility Spectrometer for Nanoparticle Measurements." *The Analyst* 142 (10): 1800–1812. <https://doi.org/10.1039/c7an00328e>.
- Chen, T., M. Liu, T. Gao, P. Cheng, S. Mei, and Y. Li. 2022. "A Fusion-Based Defogging Algorithm." *Remote Sensing* 14 (2): 425. <https://doi.org/10.3390/rs14020425>.
- Dar, K. A., and S. Mittal. 2021. "An Enhanced Adaptive Histogram Equalization Based Local Contrast Preserving Technique for HDR Images." *Paper Presented at the IOP Conference Series: Materials Science and Engineering*, Eng., Mullana, Ambala, India. <https://doi.org/10.1088/1757-899X/1022/1/012119>.
- Hautiere, N., J.-P. Tarel, D. Aubert, and E. Dumont. 2008. "Blind Contrast Enhancement Assessment by Gradient Ratioing at Visible Edges." *Image Analysis & Stereology* 27 (2): 87–95. <https://doi.org/10.5566/ias.v27.p87-95>.
- He, K., J. Sun, and X. Tang. 2011. "Single Image Haze Removal Using Dark Channel Prior." *IEEE Transactions Pattern Analysis Machine Intelligent* 33 (12): 2341–2353. <https://doi.org/10.1109/TPAMI.2010.168>.
- Huang, B., T. Liu, J. Han, and H. Haofeng. 2015. "Polarimetric Target Detection under Uneven Illumination." *Optics Express* 23 (18): 23603–23612. <https://doi.org/10.1364/oe.23.023603>.
- Ju, M., D. Zhang, and X. Wang. 2016. "Single Image Dehazing via an Improved Atmospheric Scattering Model." *The Visual Computer* 33 (12): 1613–1625. <https://doi.org/10.1007/s00371-016-1305-1>.



- Khmag, A. 2023. "Smoke Removal Technique of Industrial Scene Images Based on Second-Generation Wavelets and Dark Channel Prior Model." *Soft Computing* 27 (23): 17505–17514. <https://doi.org/10.1007/s00500-023-09204-7>.
- Khmag, A., S. A. R. Al-Haddad, A. R. Ramli, and B. Kalantar. 2017. "Single Image Dehazing Using Second-Generation Wavelet Transforms and the Mean Vector L2-Norm." *The Visual Computer* 34 (5): 675–688. <https://doi.org/10.1007/s00371-017-1406-5>.
- Liang, J., W. Zhang, L. Ren, H. Ju, and E. Qu. 2016. "Polarimetric Dehazing Method for Visibility Improvement Based on Visible and Infrared Image Fusion." *Applied Optics* 55 (29): 8221–8226. <https://doi.org/10.1364/ao.55.008221>.
- Liu, F., X. Shao, Y. Gao, B. Xiangli, P. Han, and G. Li. 2016. "Polarization Characteristics of Objects in Long-Wave Infrared Range." *Journal of the Optical Society of America A* 33 (2): 237–243. <https://doi.org/10.1364/josaa.33.000237>.
- Menglei, L., L. Xuebin, C. Jie, W. Feifei, L. Tao, C. Shengcheng, Z. Zihan, and L. Qiang. 2023. "Investigating Inversion Method for Marine Atmospheric Aerosol with Complex Refractive Index." *Laser & Optoelectronics Progress* 60 (21). <https://doi.org/10.3788/lop222921>.
- Mudge, J., and M. Virgen. 2013. "Real Time Polarimetric Dehazing." *Applied Optics* 52 (9): 1932–1938. <https://doi.org/10.1364/AO.52.001932>.
- Narasimhan, S. G., and S. K. Nayar. 2002. "Vision and the Atmosphere." *International Journal of Computer Vision* 48:233–254. <https://doi.org/10.1023/A:1016328200723>.
- Oakley, J. P., and B. L. Satherley. 1998. "Improving Image Quality in Poor Visibility Conditions Using a Physical Model for Contrast Degradation." *IEEE Transactions on Image Processing* 7 (2): 167–179. <https://doi.org/10.1109/83.660994>.
- Qi, M., Q. Hao, Q. Guan, J. Kong, and Y. Zhang. 2015. "Image Dehazing Based on Structure Preserving." *Optik* 126 (22): 3400–3406. <https://doi.org/10.1016/j.ijleo.2015.07.114>.
- Qu, Y., and Z. Zou. 2017. "Non-Sky Polarization-Based Dehazing Algorithm for Non-Specular Objects Using Polarization Difference and Global Scene Feature." *Optics Express* 25 (21): 25004–25022. <https://doi.org/10.1364/oe.25.025004>.
- Rubin, N. A., G. D'Aversa, P. Chevalier, Z. Shi, W. Ting Chen, and F. Capasso. 2019. "Matrix Fourier Optics Enables a Compact Full-Stokes Polarization Camera." *Science* 365 (6448): eaax1839. <https://doi.org/10.1126/science.aax1839>.
- Schechner, Y. Y., S. G. Narasimhan, and S. K. Nayar. 2001. "Instant Dehazing of Images Using Polarization." *Paper Presented at the Proceedings of the 2001 IEEE Computer Society Conference on Computer Vision and Pattern Recognition*, Kauai, HI, USA. <https://doi.org/10.1109/CVPR.2001.990493>.
- Schechner, Y. Y., S. G. Narasimhan, and S. K. Nayar. 2003. "Polarization-Based Vision Through Haze." *Applied Optics* 42 (3): 511–525. <https://doi.org/10.1364/AO.42.000511>.
- Sengupta, D., A. Biswas, and P. Gupta. 2020. "Non-Linear Weight Adjustment in Adaptive Gamma Correction for Image Contrast Enhancement." *Multimedia Tools & Applications* 80 (3): 3835–3862. <https://doi.org/10.1007/s11042-020-09583-1>.
- Sharma, N., V. Kumar, and S. K. Singla. 2021. "Single Image Defogging Using Deep Learning Techniques: Past, Present and Future." *Archives of Computational Methods in Engineering* 28 (7): 4449–4469. <https://doi.org/10.1007/s11831-021-09541-6>.
- Soni, B., and P. Mathur. 2020. "An Improved Image Dehazing Technique Using CLAHE and Guided Filter." *Paper Presented at the 2020 7th International Conference on Signal Processing and Integrated Networks (SPIN)*, Noida, India. <https://doi.org/10.1109/SPIN48934.2020.9071296>.
- Sun, X., and Y. Xiang. 2020. "Comparison of Transfer Function Models for Well-Aquifer System Response to Atmospheric Loading." *Canadian Journal of Fisheries and Aquatic Sciences* 590:125494. <https://doi.org/10.1016/j.jhydrol.2020.125494>.
- Treibitz, T., and Y. Y. Schechner. 2009. "Active Polarization Descattering." *IEEE Transactions on Pattern Analysis & Machine Intelligence* 31 (3): 385–399. <https://doi.org/10.1109/tpami.2008.85>.
- Vedel, M., S. Breugnot, and N. Lechocinski. 2011. "Full Stokes polarization Imaging Camera." *Paper Presented at the Polarization Science and Remote Sensing V*, San Diego, California, US. <https://doi.org/10.1117/12.892491>.

- Wang, J., M. Wan, G. Gu, W. Qian, K. Ren, Q. Huang, and Q. Chen. 2022. "Periodic Integration-Based Polarization Differential Imaging for Underwater Image Restoration." *Optics and Lasers in Engineering* 149:106785. <https://doi.org/10.1016/j.optlaseng.2021.106785>.
- Wang, W., B. Li, J. Zheng, S. Xian, and J. Wang. 2008. A Fast Multi-Scale Retinex Algorithm for Color Image Enhancement. Paper Presented at the 2008 International Conference on Wavelet Analysis and Pattern Recognition, Hong Kong, CH. <https://doi.org/10.1109/ICWAPR.2008.4635754>.
- Wang, X., J. Ouyang, Y. Wei, F. Liu, and G. Zhang. 2019. "Real-Time Vision Through Haze Based on Polarization Imaging." *Applied Sciences* 9 (1): 142. <https://doi.org/10.3390/app9010142>.
- Wang, Y., Y. Su, X. Sun, X. Hao, Y. Liu, X. Zhao, L. Hongsheng, et al. 2022. "Principle and Implementation of Stokes Vector Polarization Imaging Technology." *Applied Sciences* 12 (13): 6613. <https://doi.org/10.3390/app12136613>.
- Zhu, Y., J. Shi, Y. Yang, and G. Zeng. 2015. "Polarization Difference Ghost Imaging." *Applied Optics* 54 (6): 1279–1284. <https://doi.org/10.1364/ao.54.001279>.
- Zhuang, P., C. Li, and J. Wu. 2021. "Bayesian Retinex Underwater Image Enhancement." *Engineering Applications of Artificial Intelligence* 101:104171. <https://doi.org/10.1016/j.engappai.2021.104171>.